Hindawi
Advances in Civil Engineering
Volume 2019, Article ID 5350686, 17 pages
https://doi.org/10.1155/2019/5350686

Research Article

Influences of Water Vapor on Roof Fall Accidents in Selected Underground Coal Mines in Malawi

Umali M. Yasidu,[1,2] Yoshiaki Fujii,[1] Jun-ichi Kodama,[1] Daisuke Fukuda,[1] George J. Maneya,[2] Johnson Dandadzi,[3] and Anjula B. N. Dassanayake[4]

[1]*Faculty of Engineering, Hokkaido University, N13W8, Sapporo 060-8628, Japan*
[2]*Department of Mines, Government of Malawi, P.O. Box 251, Lilongwe, Malawi*
[3]*Mchenga Coal Mine, P. O. Box 404, Mzuzu, Malawi*
[4]*University of Moratuwa, Moratuwa 10400, Sri Lanka*

Correspondence should be addressed to Yoshiaki Fujii; fujii6299@frontier.hokudai.ac.jp

Received 12 September 2018; Accepted 30 December 2018; Published 6 February 2019

Guest Editor: Ray R. Zhang

To develop affordable countermeasures against the roof falls, the accident records of Mchenga Mine were investigated as the first step. Based on the accident records, it was found that roof falls occurred most in April and May. Humidity measurements were taken both in the underground mine and at surface, and humidity peak appeared in April. The accident occurrence and the underground humidity had a positive correlation in which no roof falls could be expected under a humidity of less than a certain value. Effect of humidity on the indirect tensile strength of the rock samples collected from the mine was investigated, and it showed that the indirect tensile strength decreased with humidity. The diffusion coefficient was measured for the rock samples collected from Mchenga Mine as well as from Kaziwiziwi Mine, and the migration of water vapor into rock mass in the roof was calculated for Mchenga case. It was clarified that the weakening of tensile strength was transmitted upward at several centimeters per day from the immediate roof. This could explain the slight difference of the accident peak in April and May from the humidity peak in April. Introducing fresh and dry outside air, if possible, will not only improve the working environment but also contribute to a decrease in roof falls.

1. Introduction

Historically, mining has been imperative to human, social, and economic development, and it is a fact that the mining industry will continue to make investments to meet the increasing needs of continuously growing modern societies. To achieve this, the mining industry should be sustainable, and safety is a key aspect that is addressed to increased production. Moving from being an agro-based economy, Malawi has in recent years ventured into mining as its alternative economic driver towards the future. There are seven coalfields spread across the country, with four coalfields of bituminous coal in the Northern Region. Currently, four underground coal mining operations are running with additional two open-pit mines in these coalfields. One of the major challenges faced by these underground mines is the occurrence of hanging roof falls. Potential roof falls in underground coal mines are a threat to the lives of miners, can damage equipment, disrupt ventilation mechanisms, and block installed emergency escape routes.

Rock falls from roof and ribs are one of the major causes of mine personnel injuries, equipment damage, and production losses [1]. The hazardous nature of roof falls can be illustrated from the statistics of mine accidents recorded and published around the world from mining countries. For example, on November 1, 2012, death of two miners and the injury of two others were reported at Kaziwiziwi Coal Mine in Malawi. Van der Merwe et al. reported in 2001 [2] that despite several years of rock engineering research and application on South African collieries, roof fall accidents continue to claim lives. It was found that the causes of the falls differed for different thickness ranges of roof falls. The

thin falls, classified as "Skin falls," accounted for approximately 70% of all fatalities. Ineffective joint support and excessive bolt spacing predominantly caused them.

In the United States, mine accident statistics indicate that during the ten-year period from 1996 to 2005, 7738 miners were injured from roof falls in underground coal, metal, nonmetal, and stone mines [3]. Coal mines showed the highest rate, that is, 1.75 roof fall injuries per 200,000 h underground work. The Mine Safety and Health Administration (MSHA) of the US reported [4] seven fatalities, 278 nonfatal-days-lost (NFDL) injuries, and 152 no-days-lost (NDL) injuries on 2006 because of roof falls in US underground coal mines. The main consequences of these accidents can be in the form of human disabilities, fatalities, production downtimes, and deterioration in industrial relations which ultimately results in economic loss to the industry.

In India, a causewise classification of fatal accidents was conducted during the period 1998 to 2010. The Directorate General of Mines Safety (DGMS) reported in 2011 [5] that 32% of the total fatal accidents occurred due to roof falls in Indian coal mines. In spite of all the precautions taken in this regard, it was revealed that the trend of fatal accidents caused by the failure of roof and sides would remain a huge problem to contain.

In a broad sense, numerous studies have been done previously to manage rock stresses and investigate roadway failures and roof behavior in underground coal mines. For example, Whittaker and Singh [6] investigated the stability of a longwall gate roadway in relation to rib pillar size using field data collected in the United Kingdom; Heidarieh-Zadeh and Smith [7] conducted a stability analysis of mine tunnels/roadways based on roadway closure data at specified distances from the tunnel excavation face; Van der Merwe et al. [2] investigated the causes of roof falls in South African collieries; and Seedsman [8] discussed the failure mechanisms of roadways. All these studies have significantly increased the understanding of strata behavior near a roadway, which is the foundation for stability prediction and optimal support design.

Over the past decades, reduction in strength and stiffness in rocks attributed to an increase in water content has been extensively researched for a large variety of rock types. It showed that the extent of the water-weakening effect is highly varied among different rock types due to considerable variations in geologic characteristics of texture and lithology. Pellet et al. [9] discussed that the stability of rock masses is largely affected by the humidity conditions, which are, for example, responsible for landslides that occur after heavy rains. This is particularly true for stratified rock masses with clay-infilled discontinuities because most of the clay minerals are highly sensitive to water.

Water vapor is entering the structure from surrounding air of certain relative humidity, and then it is transported by diffusion through the pore system of the material and adsorbed on the surface of the material [10]. Chugh and Missavage [11] studied the effect of moisture in strata control in coal mines. They summarized that moisture gain and moisture loss in coal bearing rock is related to seasonal changes in the absolute humidity of mine air. When the hot and moist surface air, drawn into the mine for ventilation, it is cooled by underground rocks and as a result, the air within rock pores loses its moisture and rock mass gains moisture. In winter, surface air temperature and humidity are lower than underground rock mass, and air travelling through the mine gains temperature and humidity. This causes mine rocks to lose moisture and thus has the drying effect.

Based on roof bolt load studies done by Aughenbaugh and Bruzewski [12], most of the roof bolt slipping occurred during high humidity months. Their studies showed that considerable amount of water was absorbed in the mine by the mine air, and most of the absorbed water was deposited on the rock, in the form of surface condensation, and a portion of this is absorbed into the rock. During winter, the natural water content of rock is considerably low, and this increases the susceptibility of rocks to gain moisture during summer. In the research done by Fujii et al. [13], the steel-arch removal test was carried out on a roadway at Kushiro Coal Mine, Japan, in May 2006. Initially, even after 15 steel arches were removed, no large roof fall occurred. The unsupported span reached 16 m without large roof falls, except for rather small falls of loosened rocks that were as large as tens of centimeters. A few months later, in August and September, humid summer air flowed into the site and dripping water was seen on the rock surface. Thereafter, several large rock falls, as large as 2 m occurred, and it was estimated that the rock mass was weakened by the humid air inflow, and as a result, the large-scale roof falls were induced.

Above studies demonstrate the effects of moisture on strata control in coal mines and mine openings. Further, they reveal the necessity to find support systems to ensure safe operations in underground coal mines. As the case studies reveal, in the mines in Malawi, it is likely that the roof rocks are weakened and then fall as a result of humid air. Therefore, the authors sought to investigate the effect of humidity on the tensile strength of coal-bearing rocks in underground coal mines in Malawi in the earlier conference paper [14]. In this paper, underground humidity data and relationship between accidents and underground humidity are added. Further, it also describes the evaluation of water vapor diffusion coefficient in roof rocks from Mchenga and Kaziwiziwi coal mines in the Livingstonia Coalfield and results of basic simulations on the vapor migration into the roof rock. Countermeasures against the roof falls in the underground mines will be proposed.

2. Humidity Levels and Mine Accidents

2.1. Mining Sites. Two underground mines, Mchenga Coal Mine (S10°42′55″, E34°9′14″) and Kaziwiziwi Coal Mine (S10°42′29″, E34°9′50″), are located in the target area hosting the Livingstonia Coalfield. The Livingstonia Basin is one of the 12 Karoo basins which are widely distributed in northern Malawi (Figure 1). Stratigraphically, the area is composed of Karoo system strata preserved in many N-S

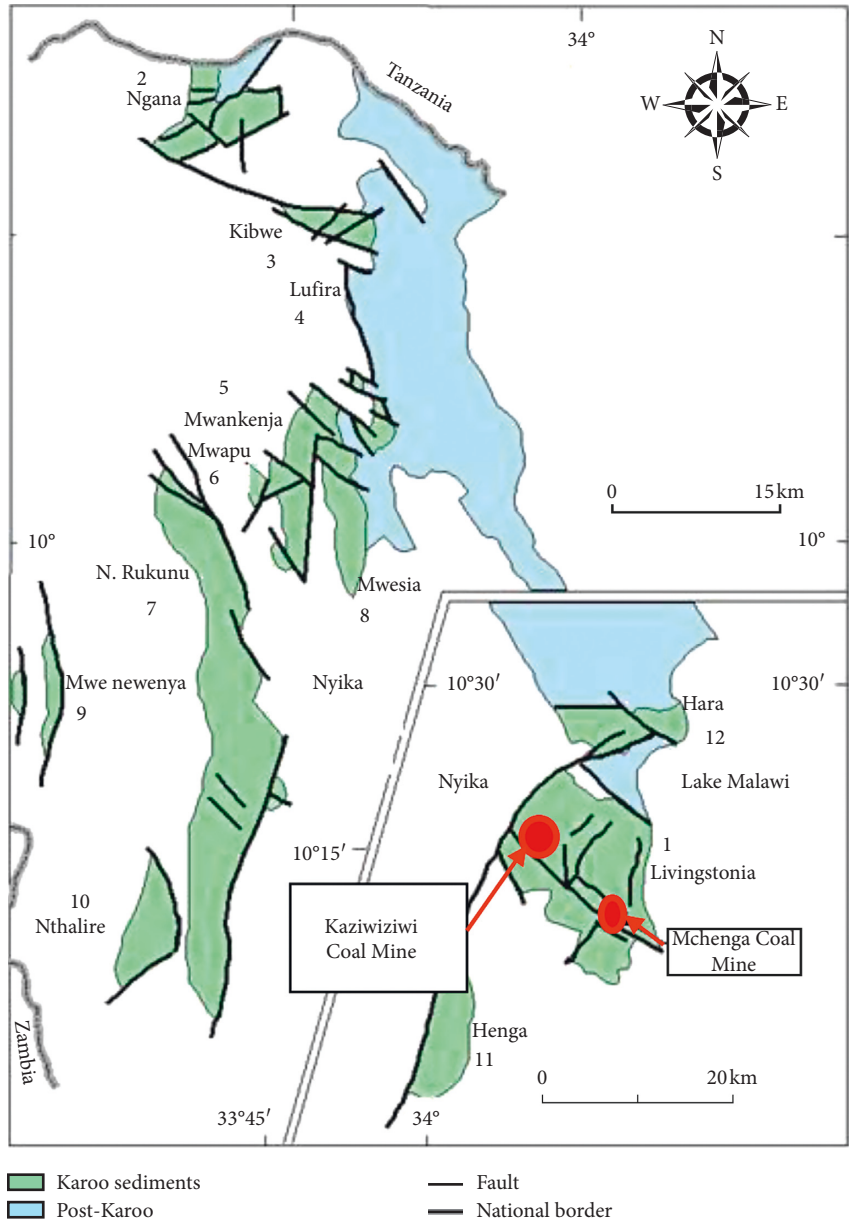

Figure 1: Distribution of Karoo basins in northern Malawi: North Nyika Basins and Livingstonia Basin (inset) based on an internal report at the Geological Survey Department in Zomba, Malawi.

trending basins and down-faulted troughs that display faulted relationship to the underlying basement complex gneisses. The basal beds of the succession consist of conglomerates and sandstones referred to the Dwyka (Carboniferous) and lower Ecca series (Permian).

These are overlain by a sequence of carbonaceous shales and coal seams commonly called coal measures of lower Ecca series (Permian) [15]. The roof stratum mainly consists of sandstone and shale of the upper Ecca group (Permian). The mines use room and pillar mining method. The annual production, pillar dimension, coal seam thickness, and maximum working depth are ca. 120 kt, 10 m × 10 m, 0.7 m to 3 m, and 150 m for Mchenga Coal Mine and ca. 80 kt, 12 m × 12 m, 1.7 m to 2.3 m, and 220 m for Kaziwiziwi Coal Mine, respectively.

2.2. Weather Conditions in the Northern Region. Malawi has two distinct seasons. From November to April is the warm-wet season during which 95% of the annual precipitation takes place (Figure 2). During January to March, the air over Malawi is moist and unstable. The daily relative humidity values range from 62% to 85% in Mzuzu at the Northern Region [16]. This is triggered by moderate to heavy rainfall ranging from 88 mm/d to 110 mm/d, confined to very few areas in the north and southern areas of Malawi. This often leads to flooding in some areas in the Northern Region. In addition to that, recorded air temperatures hovered across the region with a minimum range of 20°C to 25°C and a maximum range of 30°C to 35°C.

A cool-dry winter is evident from May to August, with a short hot-dry patch lasting from September to October.

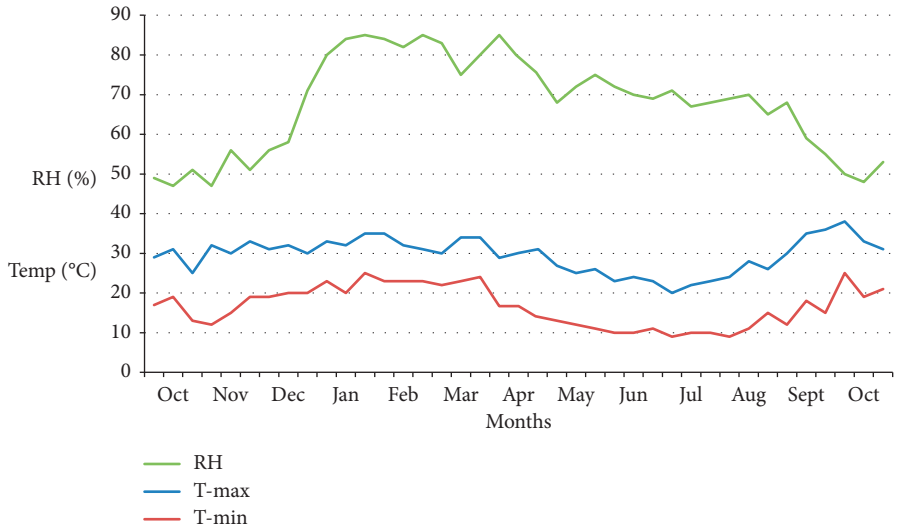

Figure 2: Relative humidity and temperature in the Northern Region, 2014-2015 season [16].

Temperatures vary from 25°C to 37°C while humidity ranges from 70% to 50% from the wetter months to dryer months, respectively. End of October marks the beginning of the rainfall season in the country, with the main rains arriving from mid-November at the southern region and progressively spreading northwards. During this period, the main rain bearing systems that influence weather over Malawi include the Intertropical Convergence Zone (ITCZ), Congo air mass, Easterly Waves, and Tropical Cyclones [17].

2.3. Average Accidents Occurrence. Mchenga Coal Mine recorded 383 accidents over a period of fourteen years (1995 to 2009) with injuries ranging from minor to severe and cases of fatal wounding leading to the death of miners. Analysis of the roof fall accidents data showed a high average number of roof fall accidents per month with a peak of severe accidents in April and May as shown in Figure 3.

Considering the scale of operations, this highly unsafe operation condition could be attributed to faulting in the rock strata coupled with the poor design of support systems, poor performance of support elements, and lack of technical know-how towards estimation of unknown nature of the stress regime existing in the mine.

2.4. Humidity Measurement. Seven, coin-type data loggers (Figure 4) were installed at varying levels in and close to the working face with an average depth of 130 m from the ground surface (Figure 5) in mine adits of Mchenga Coal Mine. The instruments were fixed in matt packs not to be damaged or stolen. Hence, there was not enough airflow. Therefore, the recorded humidity may be higher than the surrounding atmosphere. In addition, one data logger was installed at the mine office at the ground surface.

Humidity measured outside (in the mine office) showed a peak in early April (Figure 6). The humidity cycle of rising and lowering humidity levels was noticed to begin again in November clearly confirming that humidity levels are influenced by the seasonal changes of rainy-wet season and hot-dry season. Certain underground data loggers (#6, #7, and #8) failed to record the data continuously. This would be due to high humidity and less air flow in the matt packs, where condensation likely took place and water droplets accumulated on the instruments. The humidity data by other underground loggers exhibited a linearly increasing trend. This trend, which would also be due to the high humidity and less air flow, was removed so that the humidity of the starting day became equivalent to the data one year after the day. Corrected humidity readings were high, having an average of 96.9% and showed a peak at the end of April (Figure 6) while temperature readings remained steady averaging 28°C.

A correlation between the monthly averaged roof fall accidents from Mchenga Mine and the measured humidity levels by the underground logger #2 was compared (Figure 7). The number of minor and severe accidents increases with average relative humidities. From these data, it can be supposed that high humidity is an influencing factor for roof fall accidents in the underground coal mines. The 95% confidence limits for both minor and severe accidents suggest that reducing humidity levels below 84% would prevent the accidents from happening. The humidity level would be higher than the actual average level as stated above. However, Figure 7 at least suggests that affordable methods that can reduce relative humidity to a certain level would ensure the reduction of roof fall accidents in the mines.

3. Rock Samples

Rock samples were collected from the mining sites to understand the characteristics of the roof rocks in the underground coal mines. Microscopic observations were conducted on thin sections prepared from the intact rock

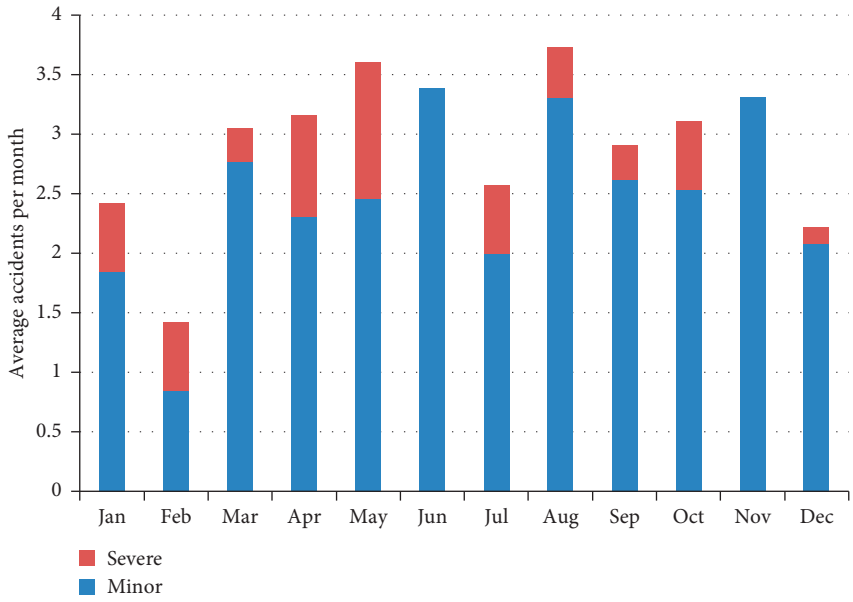

Figure 3: Average roof fall accidents per month for Mchenga Coal Mine (1995 to 2009).

Figure 4: Coin-type data logger.

blocks to identify the main mineral composition in the rocks.

3.1. Mchenga Rocks. Medium to coarse-grained arkose sandstone (hereafter called "arkose sandstone") and ultrafine to fine-grained sandstone (hereafter called "fine-grained sandstone") from Mchenga Coal Mine were observed. Scanned images of the thin sections for arkose sandstone showed no obvious open pore spaces (Figure 8(a)). It exhibited a uniform color and texture. As for the fine-grained sandstone, there were patches of different colors which could indicate different textures (Figure 8(b)). The calculated effective porosity for arkose sandstone was 6.9%, while for fine-grained sandstone it was found to be 8%.

From the microscopic images of the thin sections (Figure 9), Mchenga arkose sandstone showed a rich content of carbonate minerals and biotite. Quartz and K-feldspar particles are as large as 0.5 mm. The matrix minerals included illite, cryptocrystalline siliceous minerals, and carbonate minerals. On the other hand, the Mchenga fine-grained sandstone showed an argillaceous part lamination and a conspicuous black thick band. Quartz and K-feldspar particles are as large as 0.1 mm. The matrix minerals included illite, goethite, coaly substances, and opaque minerals.

3.2. Kaziwiziwi Rocks. Conglomerate and carbonaceous sandstone samples from Kaziwiziwi Coal Mine were also observed. The scanned image of the thin section of the conglomerate showed irregularities of minerals which indicates obvious open pore spaces (Figure 10(a)), while that of Kaziwiziwi carbonaceous sandstone exhibited a uniform color and texture (Figure 10(b)). The effective porosity for the conglomerate and the carbonaceous sandstone was 11.2% and 9.3%, respectively.

Microscopic observations and X-ray diffractions (XRD) were conducted on the rocks to identify the main minerals. Kaziwiziwi conglomerate consisted of granite fragments, muscovite, and sphalerite. The granite fragments are as large as several millimeters and consist of plagioclase, quartz, and orthoclase. The matrix was found to consist of fine particles of plagioclase, chlorite, and sericite (Figures 11(a)–11(d)). As for Kaziwiziwi carbonaceous sandstone, it was found that the apparent sedimentary structure mainly consisted of coal, quartz, and muscovite. The quartz particles are as large as 0.1 mm. It also consists of trace amount of chlorite which was probably altered from biotite (Figures 11(e)–11(h)).

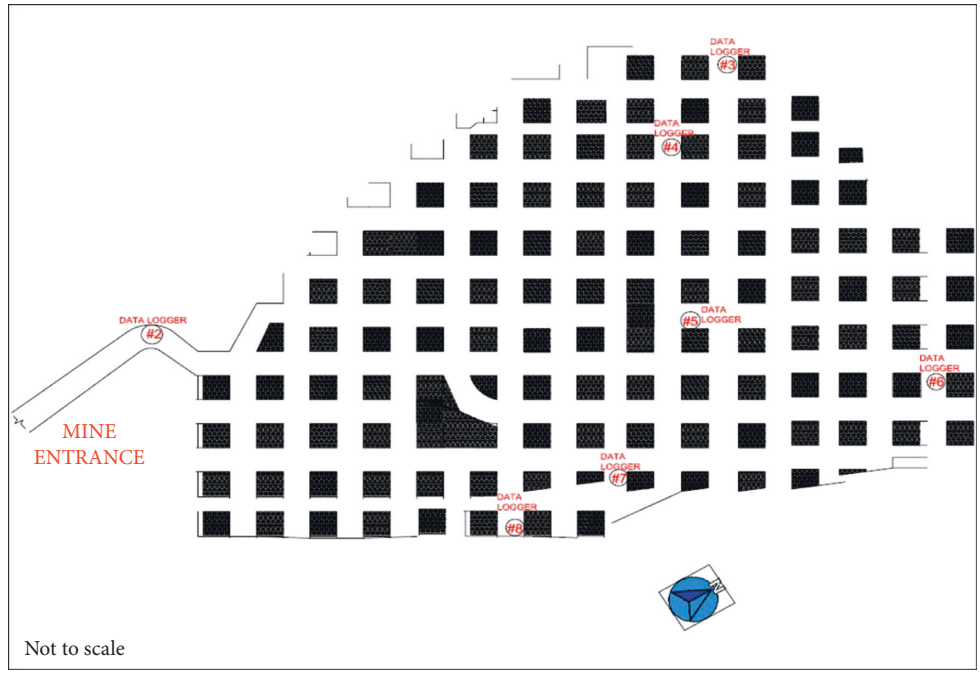

Figure 5: Location of data loggers.

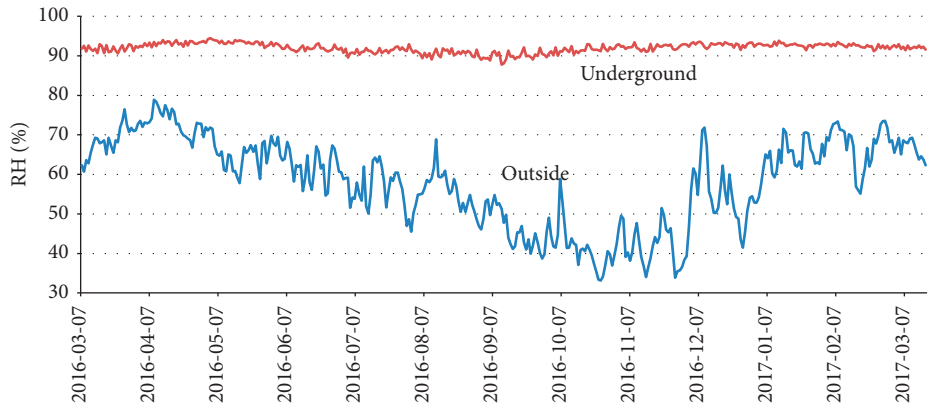

Figure 6: Humidity variation: inside the mine (logger #2) and outside.

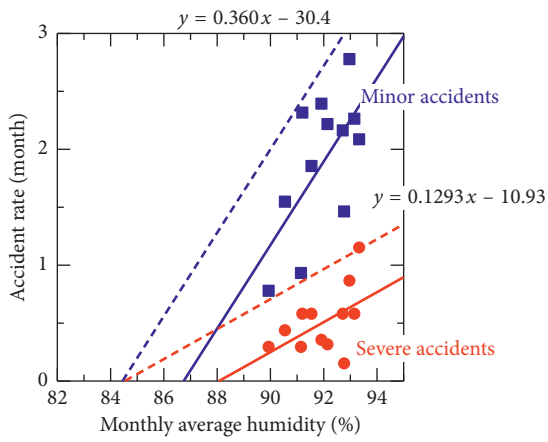

Figure 7: Relationship between accidents rate and monthly average humidity levels by data logger #2. Broken lines are the upper limits of the 95% confidence of the regression lines.

3.3. Kimachi Sandstone. In addition to above two rock types, Neogene-tuffaceous Kimachi sandstone from Japan was also examined. Kimachi sandstone is a relatively well-sorted medium-hard clastic rock with a typical grain size in the range of 0.4–1.0 mm. It consists mostly of rock fragments of andesite and crystal fragments of plagioclase, pyroxene, hornblende, biotite, and quartz, as well as calcium carbonate, iron oxides, and matrix zeolite [18]. The porosity of Kimachi sandstone was found to be ranging from 19% to 22% as discussed by Dassanayake et al. [19].

4. Effect of Humidity on Tensile Strength

4.1. Sample Preparation. Mchenga rocks (arkose sandstone and fine-grained sandstone) together with Kimachi sandstone were used for the experiments. Three sets of 25 cylindrical rock specimens (i.e., 75 specimens in total) having

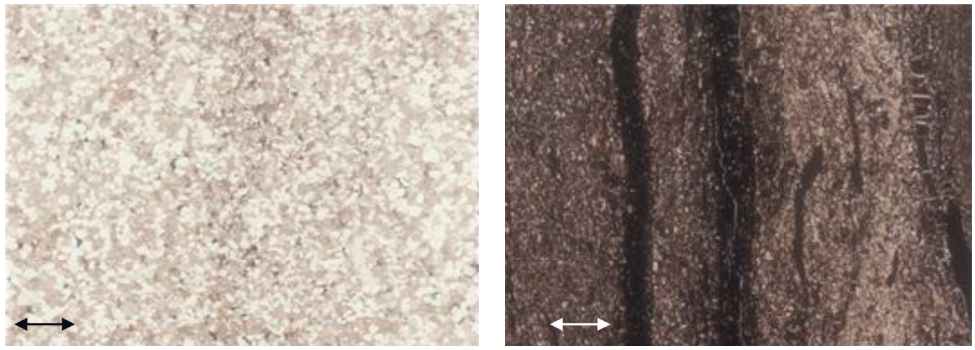

(a) (b)

Figure 8: Scanned thin section images. The arrow length is 2 mm. (a) Mchenga arkose sandstone. (b) Mchenga fine-grained sandstone.

30 mm in both length and diameter were cut from blocks of three types of rocks. The specimen ends were polished to a flatness of 0.02 mm.

Some specimens were oven dried at 80°C. To attain low humidity (2%), 400 ml of dry-up compact desiccant was used. Moderate humidity (58%) was obtained using saturated magnesium-nitrate-hexahydrate [$Mg(NO_3)_2{\cdot}6H_2O$] solution, while high humidity (98%) was achieved by pure water poured in the container. Finally, some specimens were vacuum saturated using pure water. Air-tight containers were used to maintain the applied humidity levels. The specimens were weighed and recorded daily using a balance with 1 mg resolution. This experimental setup was maintained in an isothermal condition of 22°C in the laboratory for a period of 30 days.

After preparation of the specimens, the Brazilian test, using Instron 5500R loading frame, was carried out on the specimens at a platen speed of 0.3 mm/min to calculate the indirect tensile strength using the following expression:

$$T_0 = \frac{2F_{\max}}{\pi \cdot d \cdot l}, \tag{1}$$

where T_0 is the indirect tensile strength (Pa), $F_{\max}$(N) is the maximum compressive load, d(m) is the diameter of specimen, and l (m) is the length of specimen. The load was applied parallel to the sedimentary plane.

4.2. Density Change. The change in density differed with condition of rock specimens. In all cases, the mass either increased or decreased rather rapidly in the initial stage and then almost converged with time. It was noted that arkose sandstone had higher values of density as compared to other sandstones (Figure 12). It was evident that the final bulk density of specimens increased with increase in relative humidity except for the moderate humidity of the arkose sandstone. The relationship is represented by the following expression:

$$\rho = A_d + B_d H, \tag{2}$$

where ρ(kg/m^3) is the final bulk density, H(–) is relative humidity, A_d(kg/m^3) is density at zero humidity, and B_d (kg/m^3) is the increase in density for 100% humidity (Table 1).

4.3. Indirect Tensile Strength. The oven-dried specimens showed a high compressive load which resulted in higher values of indirect tensile strength (Figure 13). In the same manner, specimens treated in low humidity (2%) had higher indirect tensile strength than those treated in moderate humidity (58%), high humidity (96%), and vacuum-saturated specimens. The subcritical crack growth (SCG [20]) is one of the main causes of the reduction of tensile strength by humidity in particular for crystalline rocks. However, the reduction of tensile strength may depend mainly on the decrease in the suction of the meniscus water between clay mineral particles [21] for sedimentary rocks.

The following equation is proposed to represent the relationship between humidity, H(–) and indirect tensile strength (MPa):

$$T_0 = A_T\left(1 - B_T\right)H, \tag{3}$$

where A_T(MPa) is the indirect tensile strength at zero humidity and B_T(–) is the sensitivity of indirect tensile strength to humidity (Table 2). The already shown observation that roof falls increase with humidity underground in Mchenga mine (Figure 7) can be explained by the decrease of the tensile strength of roof rocks with humidity.

The decrease in indirect tensile strength with increase in humidity in Mchenga arkose sandstone and fine-grained sandstone indicates a higher sensitivity (B_T) of the rocks with humidity increase (Table 2) than that for Kimachi sandstone. The greater sensitivity to humidity can be attributed to the content of illite, which is more sensitive to humidity (moisture), as the clay mineral in Mchenga rocks while Kimachi sandstone contains zeolite which is less sensitive to humidity.

Nepper-Christensen [22] suggested that many rock types containing illite are sensitive to variations in the relative humidity of the surrounding atmosphere since they shrink or swell as they give off or absorb moisture, especially in shales, which make part of the roof rocks in coal mines. Nara et al. [20] reported that the influence of the relative humidity on the crack velocity in rock was more significant when the

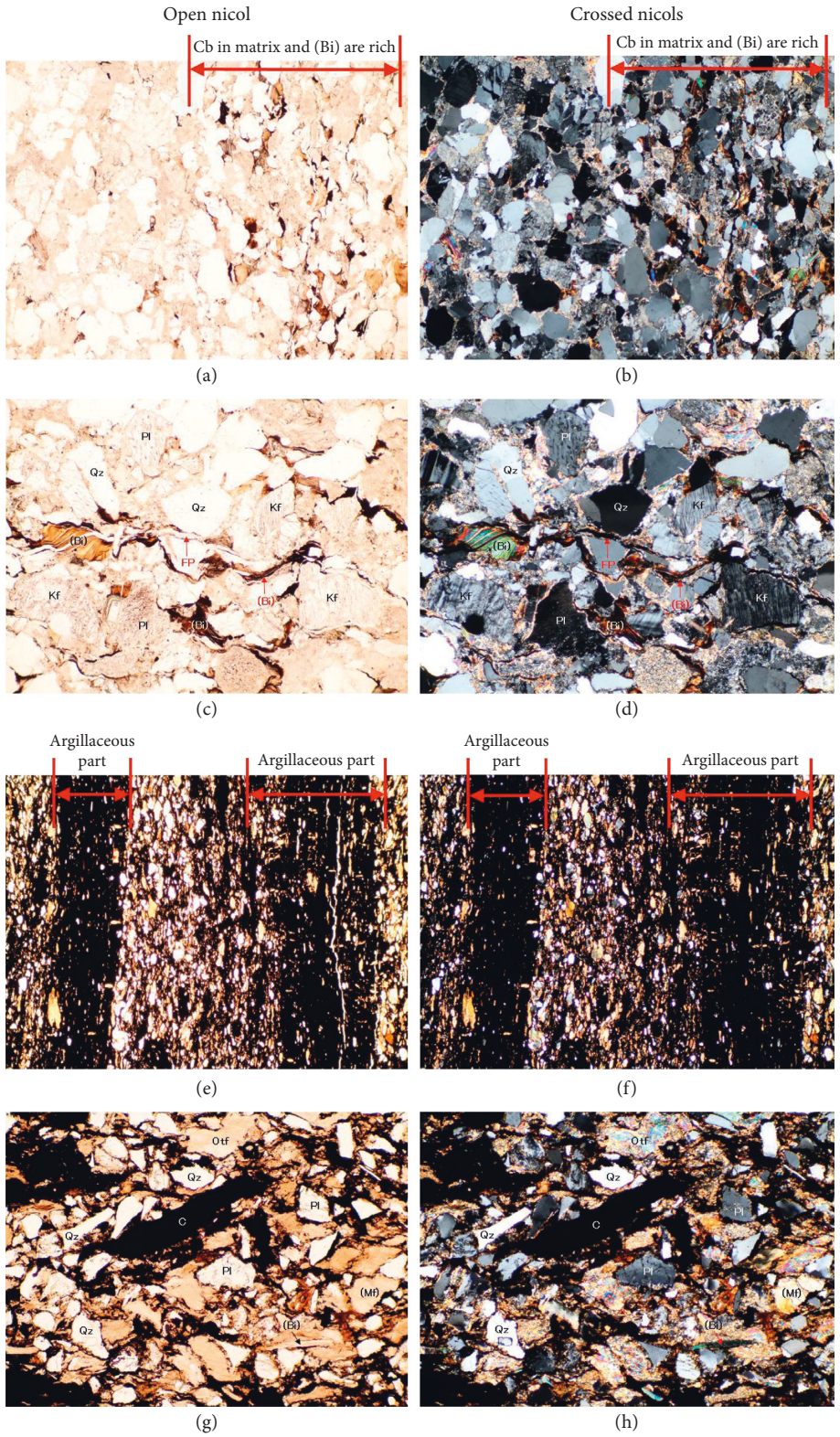

Figure 9: Microscopic images of Mchenga arkose sandstone (a, b, c, d) and Mchenga fine-grained sandstone (e, f, g, h). Qz: quartz; Kf: orthoclase; Pl: plagioclase; Bi: biotite; Mf: mafic minerals; C: coaly substances; Cb: carbonate minerals; (·): pseudomorphism; FP: fracture. Widths of the images are 6.0 mm for (a), (b), (e), and (f); 2.5 mm for (c) and (d); and 1.2 mm for (g) and (h).

rock included a larger amount of clay minerals such as smectite and illite. The results are also in tandem with the published data in other studies, which show a decrease in the mechanical properties of rocks with an increase in relative humidity, moisture content, and clay mineral content [11, 20, 23].

(a)

(b)

Figure 10: Scanned thin section images. The arrow length is 2.5 mm. (a) Kaziwiziwi conglomerate. (b) Kaziwiziwi carbonaceous sandstone.

5. Water Vapor Diffusion in Rocks

To investigate the extent of the weakened zone of rocks around the roadways with time, the rate of transport of water vapor in rocks was considered and quantified. In this section, we will present the experiments and result in the evaluation of water vapor diffusion.

5.1. Experimental Setup. Previously described Mchenga rocks, arkose sandstone and fine-grained sandstone, were used in the experiments together with carbonaceous sandstone and conglomerate from Kaziwiziwi Coal Mine. Four sets of 10 cylindrical rock specimens (i.e., 40 specimens in total), having 30 mm in both length and diameter were cut from blocks of the four rock types. The specimen ends were polished to a flatness of 0.02 mm.

Specimens were oven-dried at 80°C for a period of seven days. The dry specimens were jacketed with heat shrinkable tube to prevent vapor diffusion from the lateral sides of the specimens. The jacketed specimens were dried in the oven at 80°C for another three days. After oven drying, dry mass of the specimens was measured and recorded.

Following that, the specimens were treated in high humidity (98%) achieved by pure water. Subsequently, hourly measurements of the change in weight of the samples were carried out to determine the rate of water vapor movement through the specimen from a controlled atmosphere. The air-tight containers were used to maintain the applied humidity levels on the specimens. This experimental setup was maintained in an isothermal condition of 22°C in the laboratory for a period of 30 days.

5.2. Evaluation of Diffusion Coefficient. Vapor diffusion is a complicated thermodynamic process in the porous rock due to condensation, adsorption, chemical reactions, etc. However, it assumes here that the vapor diffusion can approximately be represented by Fick's law as

$$\frac{\partial \theta}{\partial t} = D_{\mathrm{v}} \frac{\partial^2 \theta}{\partial^2 x}, \tag{4}$$

where $\theta(\mathrm{kg/m^3})$ is the vapor density, $D_{\mathrm{v}}(\mathrm{m^2/s})$ is the diffusion coefficient, and $x(\mathrm{m})$ is the distance along the longitudinal sample axis.

Assuming θ_0 is applied at both ends of specimen at $t = 0$ and solving equation (4) under the assumption that $\theta = 0$ at $t = 0$, the following equation is obtained:

$$\theta(x,t) = \theta_0 - \frac{4\theta_0}{\pi} \sum_{n=1}^{\infty} \frac{1}{2n-1} e^{-D_{\mathrm{v}}((2n-1/l)\pi)^2 t} \sin \frac{2n-1}{l} \pi x. \tag{5}$$

Let Δm, A, and l be the change in mass (kg), sectional area ($\mathrm{m^2}$), and specimen length (m), respectively:

$$\Delta m = A \int_0^l \theta(x,t)\, dx = lA\theta_0 - A \frac{4\theta_0 l}{\pi^2} \sum_{n=1}^{\infty} \frac{1}{(2\mathrm{n}-1)^2} e^{-D_{\mathrm{v}}((2n-1/l)\pi)^2 t}. \tag{6}$$

Differentiating the equation only for $n = 1$ with respect to time,

$$\frac{d\Delta m}{dt} \cong 4lA\theta_0 \frac{D_{\mathrm{v}}}{l^2} e^{-D_{\mathrm{v}}(\pi/l)^2 t}. \tag{7}$$

Taking logarithm,

$$\ln \frac{d\Delta m}{dt} = \ln 4lA\theta_0 \frac{D_{\mathrm{v}}}{l^2} - D_{\mathrm{v}} \left(\frac{\pi}{l}\right)^2 t. \tag{8}$$

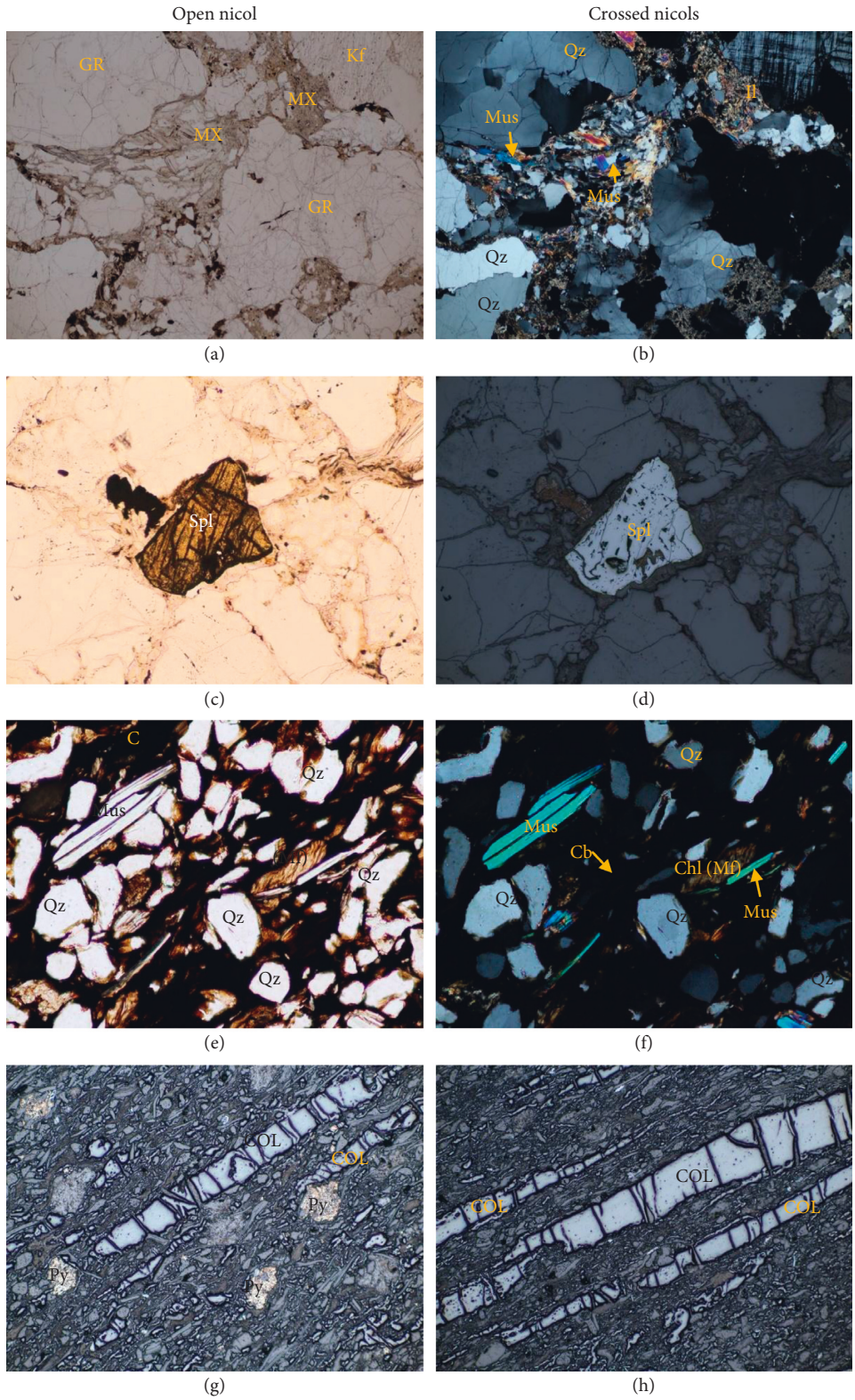

Figure 11: Microscopic images of Kaziwiziwi conglomerate (a, b, c, d) and Kaziwiziwi carbonaceous sandstone (e, f, g, h). GR: granites; MX: matrix; Mus: muscovite; Il: illite; Spl: sphalerite; Chl: chlorite; Py: pyrite; COL: coal. Widths of the images are 6.0 mm for (a) and (b); 1.2 mm for (c) and (d); 0.60 mm for (e) and (f); and 2.5 mm for (g) and (h).

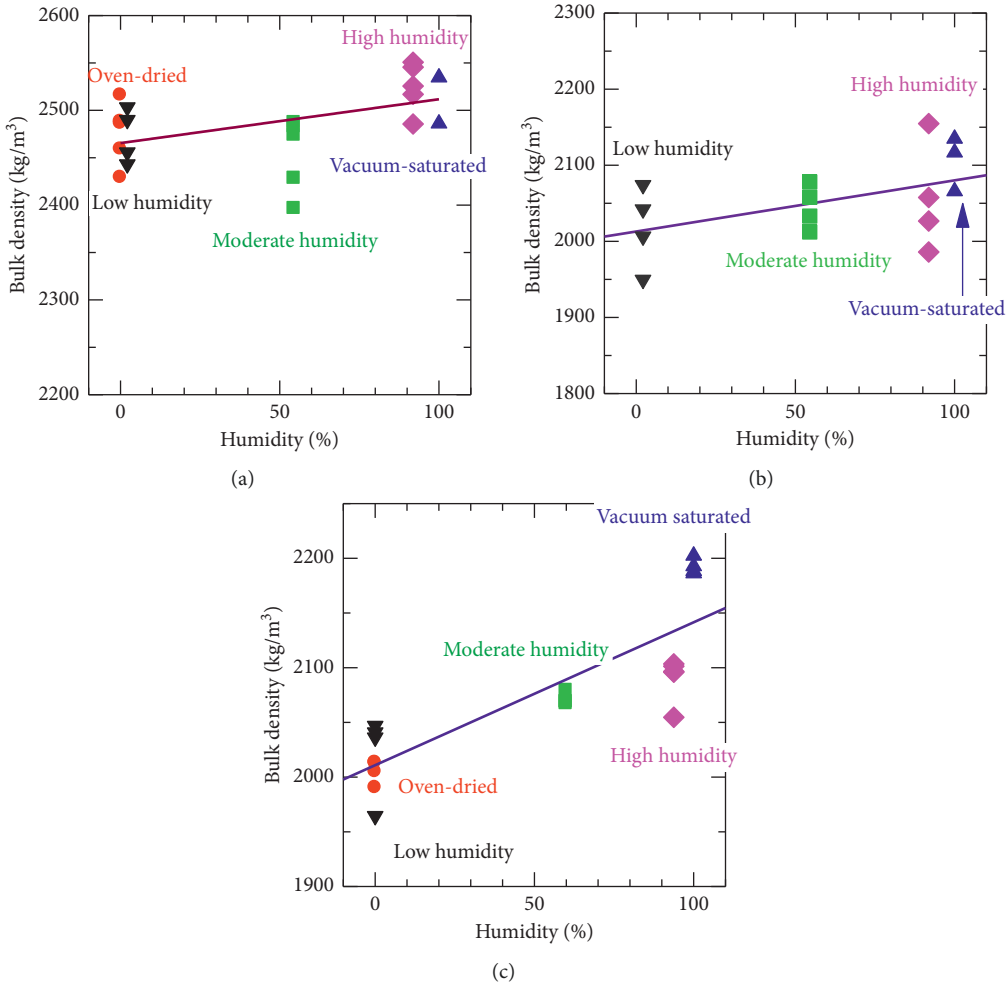

Figure 12: Bulk density variation against humidity. (a) Mchenga arkose sandstone. (b) Mchenga fine-grained sandstone. (c) Kimachi sandstone.

Table 1: Coefficients to represent density as a function of relative humidity.

	A_d (kg/m^3)	B_d (kg/m^3)
Mchenga arkose sandstone	2465	46
Mchenga fine-grained sandstone	2013	67
Kimachi sandstone	2011	131

Letting α be the slope of $\ln d(\Delta m/dt) - t$ plot,

$$\alpha = -D_v\left(\frac{\pi}{l}\right)^2, \quad \therefore D_v = -\alpha\left(\frac{1}{\pi}\right)^2. \tag{9}$$

The error due to ignoring $n \geq 2$ is less than 5% for the experimental condition.

5.3. Results. The mass increased rather rapidly in the initial stage and then almost converged. It was noted that arkose sandstone specimens generally had higher values of mass change as compared to other fine-grained sandstones for the Mchenga rocks. Water vapor diffusion coefficient was calculated using equation (9). The gradient α was calculated as the gradient of the regression line from the $\ln d(\Delta m/dt) - t$ graph (Figure 14) ignoring the initial flat part. The flat part may have appeared due to the limitation of the volume of airflow in the container.

Average diffusion coefficient for Mchenga arkose sandstone was 1.02×10^{-9} m^2/s, while it was 1.20×10^{-9} m^2/s for fine-grained sandstone. For Kaziwiziwi conglomerate and carbonaceous sandstone, the average diffusion coefficients were 1.12×10^{-9} m^2/s and 0.60×10^{-9} m^2/s, respectively. The experimentally determined water vapor diffusion coefficients increased with porosity for the rock types in each mine (Figure 15).

6. One-Dimensional FEM Simulation

To get a better insight into the behavior of the water vapor diffusion around the roadways in the underground coal mines, a numerical simulation of one-dimensional water vapor diffusion into a rock mass with sandstone was carried out using two-dimensional FE (finite element)

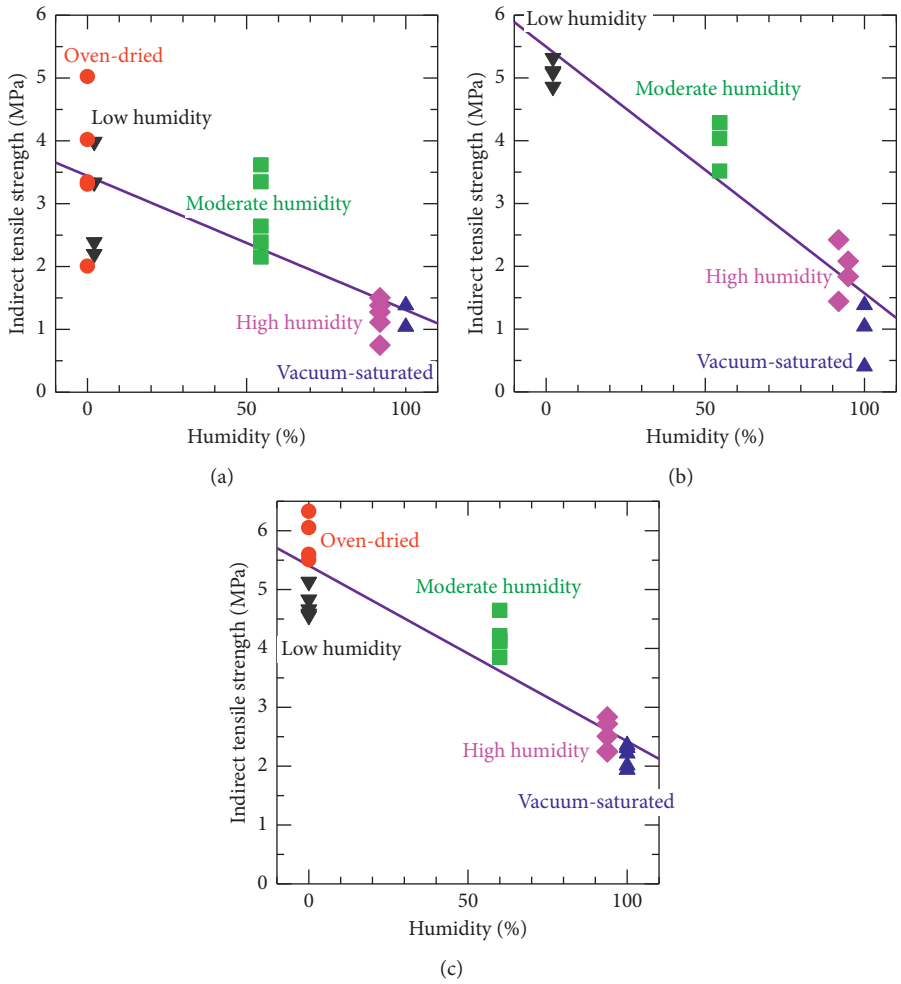

Figure 13: Indirect tensile strength variation against humidity. (a) Mchenga arkose sandstone. (b) Mchenga fine-grained sandstone. (c) Kimachi sandstone.

Table 2: Coefficients in equation (3) for three types of rocks.

Rock	Constants	
	A_T (MPa)	B_T (–)
Mchenga arkose sandstone	3.44	0.62
Mchenga fine-grained sandstone	5.50	0.71
Kimachi sandstone	5.42	0.55

code. The FE code was originally built for heat analysis [24]. However, replacing temperature and $\lambda/(\rho \cdot C)$, where λ and C are heat conductivity and specific heat, respectively, by vapor density and D_v (equation (4)), vapor diffusion can be calculated.

A simple two-dimensional finite element mesh of 0.1 m × 5 m (100 triangular elements, 102 nodes) was generated, as shown in Figure 16. The roof rock mass consisting of Mchenga arkose sandstone was considered homogeneous and isotropic. The longitudinal sides and top side of the elements were assumed to be impermeable, leaving the bottom side permeable.

By considering the variation of humidity conditions in the mine and outside the mine, the observed humidity data were smoothed and converted to density with the aid of equation (2). From this density value, vapor density θ was calculated from the expression $\theta = B_d H$. Change in vapor density $\Delta\theta = \theta - \theta\ (t = 0)$ was calculated for underground conditions (Figure 17(a)) and outside condition (Figure 17(b)), respectively, and $\Delta\theta$ was applied at the bottom boundary with water vapor diffusion coefficient D_v as 1.02×10^{-9} m^2/s.

6.1. Response to a Step Function. Before showing the response to the measured humidity change, delayed migration of water vapor into the roof rock was simulated (Figure 18(a)) applying vapor density which increased instantaneously from 0 to 100% at $t = 0$ and remained constant for the whole duration. At depth of 1 m, density change increased rapidly followed by a steady increase. In the intermediate layer, represented by the depth of 3 m and 5 m, there was a uniform increase with a lag, and finally, the change appeared at the depth of 10 meters. The migration and adsorption of this water vapor resulted in a delayed weakening of the rocks with depth (Figure 18(b)).

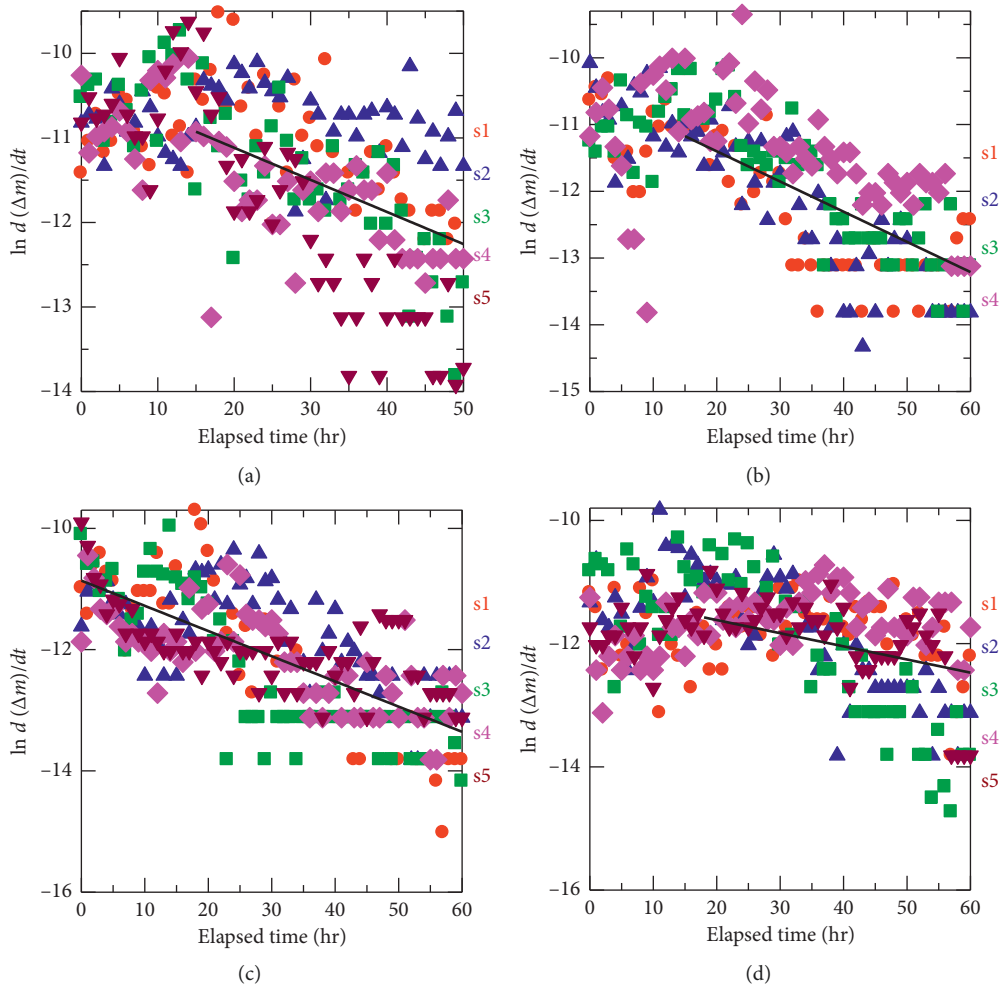

FIGURE 14: Mass change of specimens as a function of elapsed time. The thick black line gives the regression line to calculate average diffusion coefficient. (a) Mchenga arkose sandstone. (b) Mchenga fine-grained sandstone. (c) Kaziwiziwi conglomerate. (d) Kaziwiziwi carbonaceous sandstone.

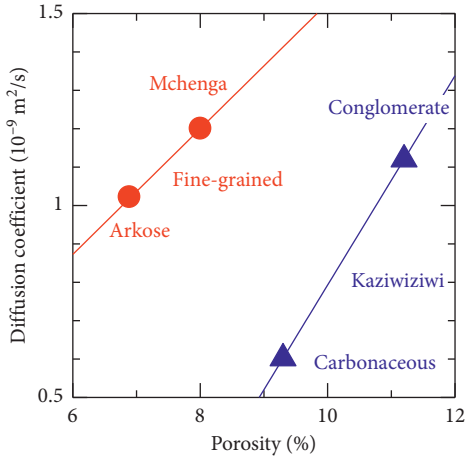

FIGURE 15: Dependence of water vapor diffusion coefficients of Malawi rocks on porosity.

6.2. Response to Annual Variation. The calculation was carried out for two years, and the result for the second year, which was considered not to be affected by the initial water vapor, was only shown in here. For underground conditions, simulation results with a 30-day delay from the immediate layer at 1 m depth indicated a drop of indirect tensile strength by several percent (Figure 19(a)). When considering outside conditions, the results showed a drop of indirect tensile strength by several 10 percent at 1 m depth with a delay of 20 days (Figure 19(b)). In other words, the peak of the minimum tensile strength is transmitted upward with a delay of several centimeters per day from the immediate roof.

Due to insufficient airflow in the matt packs in which underground data loggers were installed, it was assumed that the prevailing humidity values in the coal mine could be between underground and outside values, and the decrease in tensile strength would be between several percent and several ten percent. The calculated decrease in tensile strength is for the sedimentary planes in the rock specimens and would be larger than the weak sedimentary planes which cause roof falls. However, the ratios of the estimated decrease amount to the average strengths of weak sedimentary planes would not be far from that for the sedimentary planes

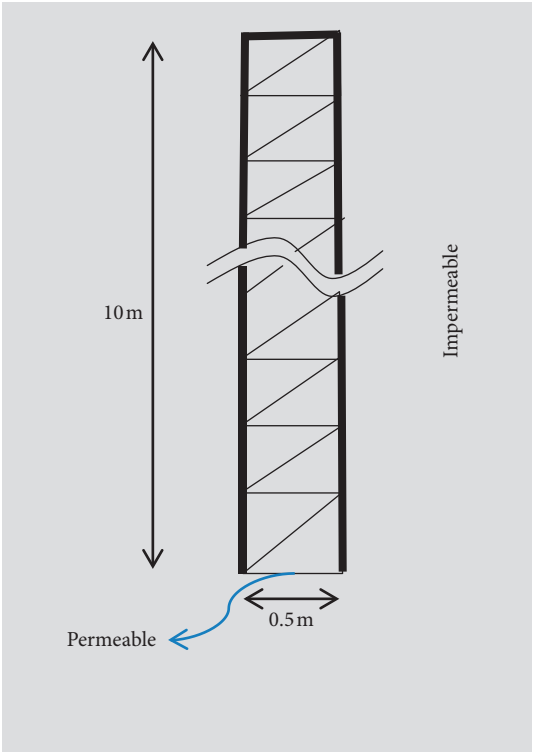

Figure 16: Finite element mesh configuration used in numerical simulation. The top and side boundaries are impermeable; bottom side is permeable.

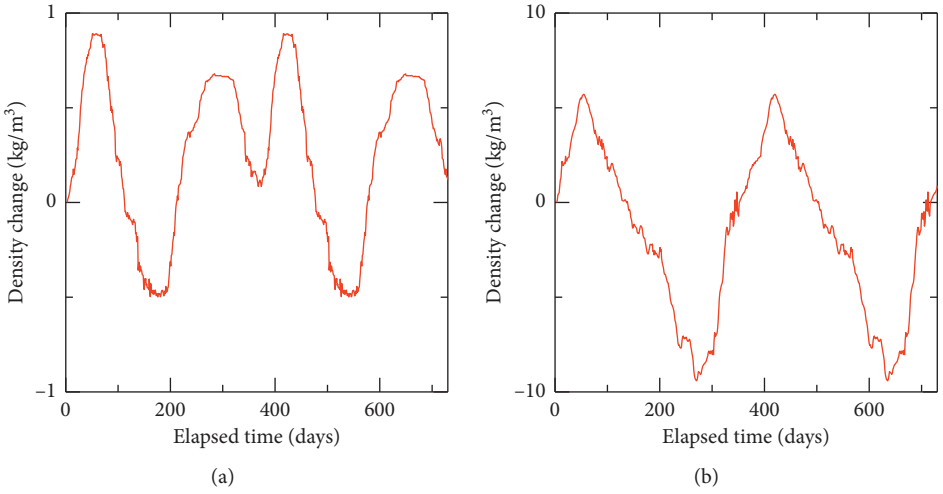

Figure 17: Density change for FEM simulation converted from smoothed humidity data. Time is from February 15. (a) Underground conditions. (b) Outside conditions.

in the rock specimens. Therefore, it can be concluded that tensile failure at weak sedimentary planes due to the seasonal decrease in tensile strength by the vapor migration into the rock mass would have been playing an important role for the roof falls at Malawian coal mines.

The recorded severe accident peak is in April and May. The peak is slightly delayed from the peak of the measured humidity peak in April. Considering the thickness of the typical roof falls in the mines is of skin falls with the thickness of several centimeters to several 10 cm, this slight difference between the peak humidity and peak accident occurrence may be explained by possible delay for the migration of vapor into the rocks, which weakens them.

Seepage of rainwater into roadways could be assumed as one of the causes for roof fall mechanisms at shallow coal mines. The delay of the peak occurrences of accident from the rainy season can be explained by the assumption. However, rock weakening seems to extend upward from the roadway roof because most roof falls are of skin falls. This would suggest that the migration of water vapor is more

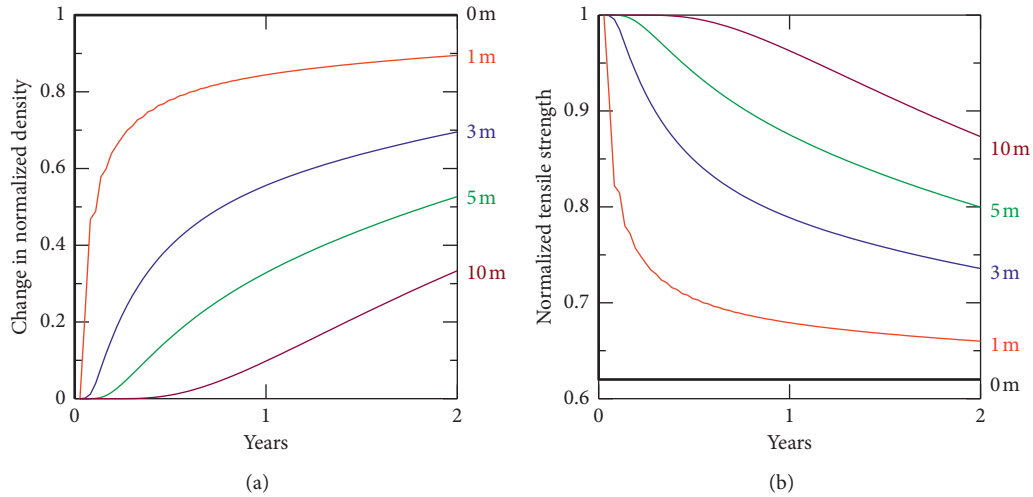

Figure 18: Response to a step humidity increase from 0 to 100%. (a) Delayed migration of density change. (b) Delayed weakening of roof rocks.

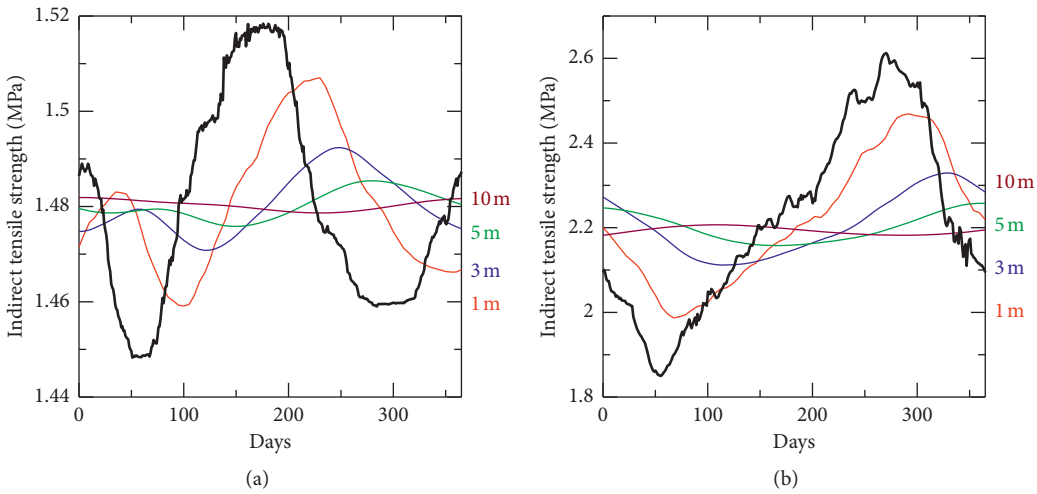

Figure 19: Simulation of annual variation. Time is from February 15. The thick black lines show the boundary condition at the bottom. (a) Underground. (b) Outside.

likely to be the main cause of roof falls than seepage of rainwater, which is from the ground surface to the roadway roof.

7. Countermeasure to Decrease Roof Fall Accidents

Severe compressive stress concentrations, which are often the main cause of rock failure in deep mining, cannot be the main cause of the roof falls in the shallow Malawian mines. Instead, the tensile failure by the gravity force at the weak sedimentary planes which are even more weakened by water vapor diffusion from rock surface would be the main cause of the skin falls. The accidents can certainly be prevented if the number of rock bolts and steel meshes were increased considerably. However, the mining companies cannot afford expensive measures because the scale of the mining is very small and not so profitable.

The cause of the high humidity in the mines is due to the natural ventilation adopted there. Introducing fresh and dry outside air into the mine adits by installing a mechanized ventilation system is proposed here as a less expensive countermeasure than increasing rock bolts and steel meshes. The outside dry air could increase the tensile strength of weak sedimentary planes and prevent roof falls. Rockbolts and steel meshes only prevent roof falls where they are installed and will be left in place. On the other hand, the mechanized ventilation system would work for the entire mine areas for a longer time and not only prevent roof falls but also significantly improve the working environment.

8. Conclusions

Roof fall is one of the major problems in Malawian underground coal mines. To develop affordable countermeasures against the roof falls, the accident records of Mchenga Mine

were investigated as the first step. Based on the accident records, it was found that roof falls occurred mostly in April and May. Humidity measurements were taken both in the underground mine and at surface, and the humidity peak appeared in April. The accident occurrence and the underground humidity had a positive correlation in which no roof falls could be expected under a humidity of less than a certain value. Effect of humidity on the indirect tensile strength of the rock samples collected from the mine was investigated, and it showed that the indirect tensile strength decreased with humidity. The diffusion coefficient was measured for the rock samples collected from the Mchenga Mine as well as from Kaziwiziwi Mine, and the migration of water vapor into the roof rock mass was calculated for the Mchenga case. It was clarified that the weakening of tensile strength was transmitted upward at several centimeters per day from the immediate roof, and this could explain the slight difference of the accident peak in April and May from the humidity peak in April. Introducing fresh and dry outside air, if possible, will not only improve the working environment but also contribute to a decrease in roof falls. 2D FEM analysis may explain the extent of weakened zones around a roadway in underground coal mines in future.

Data Availability

The humidity data used to support the findings of this study are available from the corresponding author upon request.

Conflicts of Interest

The authors declare that they have no conflicts of interest.

Acknowledgments

The authors appreciate Mchenga Coal Mine Management, engineers, and staff for their cooperation in conducting this study. This research was supported by JICA under KIZUNA Program (J-15-10275).

References

[1] B. Shen, "Coal mine roadway stability in soft rock: a case study," *Rock Mechanics and Rock Engineering*, vol. 47, no. 6, pp. 2225–2238, 2013.

[2] J. N. van der Merwe, J. J. van Vuuren, R. Butcher et al., "Causes of falls of roof in South African collieries," *Safety in Mines Research Advisory Committee (SIMRAC)*, Final project report, report no. COL613, SciELO Network, Johannesburg, South Africa, 2001.

[3] Mine Safety and Health Administration (MSHA), *Quarterly Employment and Production: Accidents/Injuries/Illnesses Reported to MSHA under 30 CFR Part 50*, US Department of Labour, Mine Safety and Health Administration, Office of Injury and Employment Information, Crystal City, VA, USA, 2005.

[4] Mine Safety and Health Administration (MSHA), 2018, https://www.msha.gov/data-reports/statistics.

[5] Directorate General of Mines Safety, Dhanbad, India, "Fatal accidents in coal mines," *DGMS Strategic Plan*, vol. 15, pp. 26-27, 2011.

[6] B. N. Whittaker and R. N. Singh, "Stability of Longwall mining gate roadways in relation to rib pillar size," *International Journal of Rock Mechanics and Mining Sciences & Geomechanics Abstracts*, vol. 18, no. 4, pp. 331–334, 1981.

[7] A. M. Heidarieh-Zadeh and S. F. Smith, "Stability behaviour of deep level coal mining tunnels," *Mining Science and Technology*, vol. 2, no. 3, pp. 171–179, 1985.

[8] R. W. Seedsman, "Geotechnical sedimentology-its use in underground coal mining," *International Journal of Coal Geology*, vol. 45, no. 2–3, pp. 147–153, 2001.

[9] F. L. Pellet, M. Keshavarz, and M. Boulon, "Influence of humidity conditions on shear strength of clay rock discontinuities," *Engineering Geology*, vol. 157, pp. 33–38, 2013.

[10] M. Keppert, J. Žumár, M. Čáchová et al., "Water vapor diffusion and adsorption of sandstones: influence of rock texture and composition," *Advances in Materials Science and Engineering*, vol. 2016, Article ID 8039748, 7 pages, 2016.

[11] Y. P. Chugh and R. A. Missavage, "Effects of moisture on strata control in coal mines," *Engineering Geology*, vol. 17, no. 4, pp. 241–255, 1981.

[12] N. B. Aughenbaugh and R. F. Bruzewski, "Investigation of the failure of roofs in coal mines," Final Report, U.S.B.M. Contract No.H0111462, University of Missouri, Rolla, MO, USA, 1973.

[13] Y. Fujii, Y. Ishijima, Y. Ichihara et al., "Mechanical properties of abandoned and closed roadways in the Kushiro Coal Mine, Japan," *International Journal of Rock Mechanics and Mining Sciences*, vol. 48, no. 4, pp. 585–596, 2011.

[14] U. M. Yasidu, Y. Fujii, D. Fukuda, J. Kodama, and G. Maneya, "Effect of humidity on tensile strength of rocks in selected underground coal mines in Malawi," in *Proceedings of US Rock Mechanics/Geomechanics Symposium 2017 (ARMA 2017)*, pp. 17–217, San Francisco, CA, USA, June 2017.

[15] G. G. W. Cooper and F. Habgood, "The geology of Livingstonia coalfield," in *Nyasaland Geological Survey Department Bulletin*, no. 11, Government Printer, Zomba, Malawi, 1959.

[16] Department of Climate Change & Meteorological Services-Malawi, "Weather and agro-meteorological bulletin–March 2015. Prospects for the 2014/2015 rainfall season in Malawi," Department of Climate Change & Meteorological Services-Malawi, Lilongwe, Malawi, 2018, http://www.metmalawi.com/bulletins.

[17] Department of Climate Change and Meteorological Services, Malawi, "Prospects for the 2017/2018 rain fall season in Malawi," Department of Climate Change and Meteorological Services, Lilongwe, Malawi, 2018, http://www.metmalawi.com/news/php.

[18] G. Dhakal, T. Yoneda, M. Kato, and K. Kaneko, "Slake durability and mineralogical properties of some pyroclastic and sedimentary rocks," *Engineering Geology*, vol. 65, no. 1, pp. 31–45, 2002.

[19] A. B. N. Dassanayake, Y. Fujii, D. Fukuda, and J.-I. Kodama, "A new approach to evaluate effective stress coefficient for strength in Kimachi sandstone," *Journal of Petroleum Science and Engineering*, vol. 131, pp. 70–79, 2015.

[20] Y. Nara, K. Morimoto, T. Yoneda, N. Hiroyoshi, and K. Kaneko, "Effects of humidity and temperature on subcritical crack growth in sandstone," *International Journal of Solids and Structures*, vol. 48, no. 7-8, pp. 1130–1140, 2011.

[21] A. K. K. So, M. Osada, M. Takahashi et al., "Characterization of drying-induced deformation behaviour of Opalinus Clay and tuff in no-stress regime," *Environmental Geology*, vol. 58, no. 6, pp. 1215–1225, 2009.

[22] P. Nepper-Christensen, "Shrinkage and swelling of rocks due to moisture movements," *Medd. fra Dansk Geol. Forening. København*, vol. 15, 1965.
[23] D. Li, L. N. Y. Wong, G. Liu, and X. Zhang, "Influence of water content and anisotropy on the strength and deformability of low porosity meta-sedimentary rocks under triaxial compression," *Engineering Geology*, vol. 126, pp. 46–66, 2012.
[24] A. Mufundirwa, Y. Fujii, N. Kodama, and J.-I. Kodama, "Analysis of natural rock slope deformations under temperature variation: a case from a cool temperate region in Japan," *Cold Regions Science and Technology*, vol. 65, no. 3, pp. 488–500, 2011.